ACS MEASUREMENT SCIENCE Au
AN OPEN ACCESS JOURNAL OF THE AMERICAN CHEMICAL SOCIETY

pubs.acs.org/measureau

Article

Total Luminescence Spectroscopy for Quantification of Temperature Effects on Photophysical Properties of Photoluminescent Materials

Max Wamsley, Weiyu Peng, Weinan Tan, Pathum Wathudura, Xin Cui, Shengli Zou, and Dongmao Zhang*

Cite This: *ACS Meas. Sci. Au* 2023, 3, 10–20

Read Online

ACCESS | Metrics & More | Article Recommendations | Supporting Information

ABSTRACT: Quantification of the temperature effects on the optical properties of photoluminescent (PL) materials is important for a fundamental understanding of both materials optical processes and rational PL materials design and applications. However, existing techniques for studying the temperature effects are limited in their information content. Reported herein is a temperature-dependent total photoluminescence (TPL) spectroscopy technique for probing the temperature dependence of materials optical properties. When used in combination with UV−vis measurements, this TPL method enables experimental quantification of temperature effects on fluorophore fluorescence intensity and quantum yield at any combination of excitation and detection wavelengths, including the fluorophore Stokes-shifted and anti-Stokes-shifted fluorescence. All model polyaromatic hydrocarbon (PAH) and xanthene fluorophores exhibited a strong excitation- and emission-wavelength dependence in their temperature effects. However, the heavy-atom effects used for explaining the strong temperature dependence of brominated anthracenes are not operative with xanthene fluorophores that have heavy atom substitutions. The insights from TPL measurements are important not only for enhancing the fundamental understandings of the materials photophysical properties but also for rational measurement design for applications where the temperature sensitivity of the fluorophore fluorescence is critical. An example application is demonstrated for developing a sensitive and robust ratiometric fluorescence thermometric method for *in situ* real-time monitoring of sample temperatures inside a fluorescence cuvette placed in a temperature-controlled sample holder.

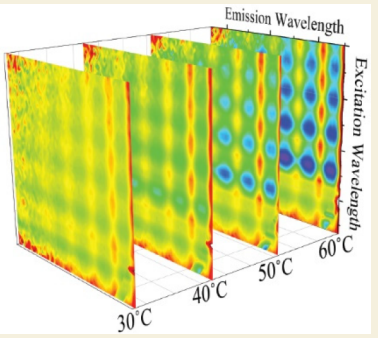

KEYWORDS: *Fluorescence, Temperature effect, Total photoluminescence, EEM, Quantum yield*

INTRODUCTION

Quantification of the temperature effects on the optical properties of photoluminescent (PL) materials is important for a fundamental understanding of both materials optical processes and rational PL materials design and applications. Mechanistically, the temperature effects on PL have been mostly attributed to the temperature dependent kinetics of the radiative and nonradiative relaxations. Example nonradiative relaxations include internal conversion, external conversion, intersystem crossing, the confinement energy of electrons, exciton binding energy, and electron−phonon interactions.[1−7] It has been generally believed that fluorescence intensity decreases with increasing sample temperature. However, a reverse temperature effect, increasing intensity with increasing temperature, has also been observed.[8−14] Multiple hypotheses have been proposed for the fluorescence signal reduction at elevated temperatures including exciplex formation, enhanced dynamic quenching, intersystem crossing, and internal conversion.[15−19] However, pinpointing the key mechanism responsible for the temperature effects on specific fluorophores remains a significant theoretical and experimental challenge.

Understanding the temperature effects on the PL materials' optical properties is also important for fluorophore applications in photovoltaics, photoluminescent displays,[7,20−22] chemical quantifications,[23−26] and fluorescence thermometry.[8−10,27,28] For applications such as photovoltaics, displays, and chemical quantification, temperature-insensitive PL materials are desirable for their performance stability against environmental temperature fluctuations. On the other hand, for thermometric measurements, PL materials with high temperature sensitivity are preferable.

Despite growing interests on the temperature effects on fluorophore fluorescence properties, there are limitations with current measurement strategies and data analysis methods. First, most existing studies are typically performed with emission spectra excited with one or two excitation wavelengths,[5−7,29−33] and the temperature effects are investigated based on the fluorescence intensity at one or two emission wavelengths. Such an approach makes it difficult to evaluate

Received: July 13, 2022
Revised: September 7, 2022
Accepted: September 8, 2022
Published: September 21, 2022

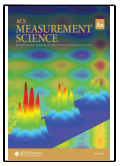

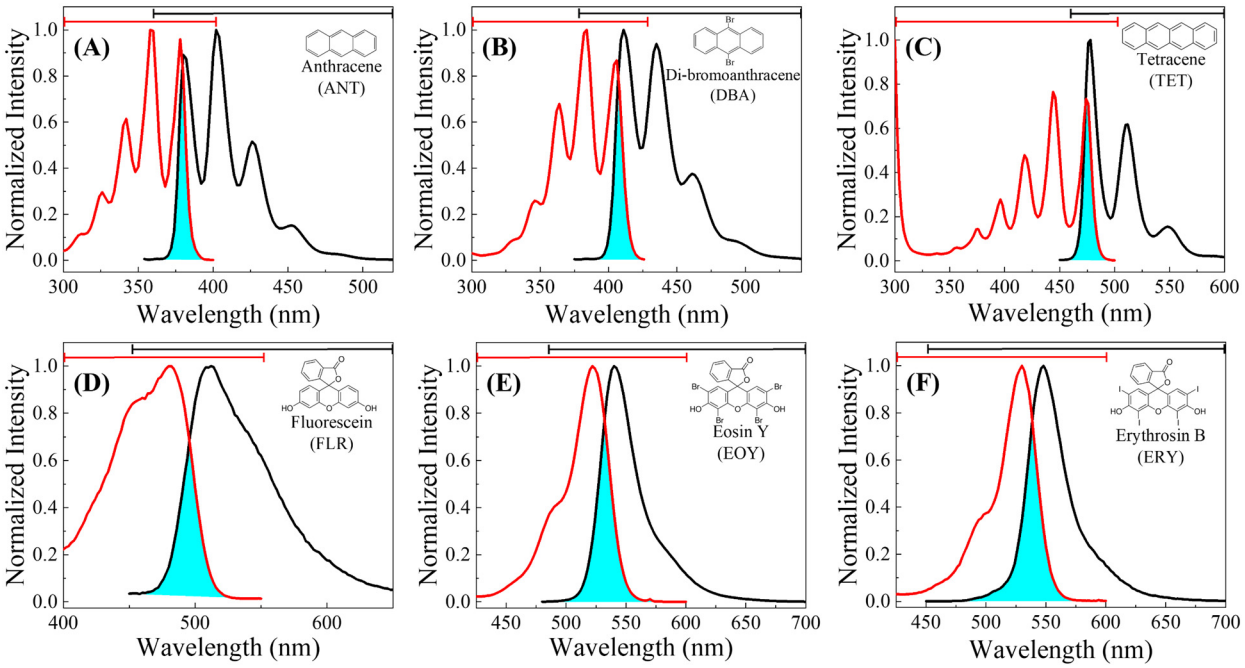

Figure 1. Structure, name, abbreviation, and fluorescence excitation and emission spectra of (A) ANT, (B) DBA, (C) TET, (D)FLR, (E) EOY, and (F) ERY. Highlighted in blue is the excitation wavelength region where the fluorophores are simultaneously ASSF-, ORF-, and SSF-active.

the general applicability of the conclusions to the data obtained with other emission and/or excitation wavelengths. Second, many studies explicitly or implicitly attribute the temperature-induced emission intensity change to the variation in the fluorophore fluorescence quantum yield (QY).[34−38] The possible temperature effects on the sample light absorption are not considered. This approach can lead to questionable conclusions because the fluorophore emission intensity is related to both its fluorescence QY and its light absorption in a rather complex manner, as shown in a recently developed first-principle model.[39] Third, the existing literature has been predominantly focused on the temperature effects at the fluorophore Stokes-shifted fluorescence (SSF). A few recent works have been devoted to the temperature effects on anti-Stokes-shifted fluorescence (ASSF).[40−45] However, to our knowledge, there is no side-by-side comparison of the temperature effects on the SSF and ASSF of the same fluorophores. Such study can be important for understanding the origins and utilities of ASSF. Lastly, most of the literature involves fluorophores dissolved in solutions, or dispersed in a solid matrix.[46−50] Side-by-side comparisons of temperature effects on fluorophores dispersed in a solid matrix and in solution are scant. Such a study would provide insights to the importance of the sample matrix.

Presented herein is a total photoluminescence (TPL), which is also commonly termed as excitation−emission matrices (EEM), spectroscopic method for experimental quantification of the temperature effects of fluorophore photophysical properties. TPL is a three-dimensional spectroscopic technique that acquires a PL spectrum at each excitation wavelength across the entire sample absorption wavelength region. A complete TPL data set is composed of the emission intensity as a function of every combination of excitation and emission wavelengths, including the regions where the emission wavelength is lower than, equal to, or longer than the excitation wavelengths. As such, the TPL enables simultaneous acquisition of the sample ASSF, SSF, and on-resonance fluorescence (ORF). The latter refers to the fluorescence with the emission wavelength identical to the excitation wavelength.[51] The fluorophores are simultaneously ASSF-, ORF-, and SSF-active when they are excited at the wavelength region where the fluorophore emission and excitation spectra overlap (Figure 1).[51]

The use of the TPL method for studying the temperature effects on the optical properties of PL materials is inspired by our recent work performed with anthracene (ANT).[39] This earlier work showed that the temperature effect on ANT fluorescence depends on the employed excitation and emission wavelengths. However, the general applicability of the conclusion is unknown because ANT is the only fluorophore used, and only four excitation wavelengths were employed for fluorescence excitation. The TPL method presented in this work enabled us to provide the global wavelength dependence with all six model fluorophores, including three polyaromatic hydrocarbons (PAHs)—ANT, tetracene (TET), and dibromoanthracene (DBA)—and three xanthene fluorophores—fluorescein (FLR), eosin Y (EOY), and erythrosine B (ERY) (Figure 1). This relatively large-scale study allows us to investigate (1) the generality of wavelength dependence of the temperature effects on fluorophore optical properties, (2) the possible difference in the temperature effects on fluorophore ASSF and SSF, and (3) the significance of heavy-atom effects in governing the temperature effect on fluorophore fluorescence. Heavy-atom effects have been proposed as the key mechanism for the strong temperature dependence of the fluorescence emission of brominated anthracenes. Since FLR, EOY, and ERY differ only in their heavy atom contents (Figure 1), one would expect ERY fluorescence to decrease faster than EOY, which would be faster than FLR, if the heavy-atom effect is indeed dominating the temperature effects on fluorophore fluorescence.

https://doi.org/10.1021/acsmeasuresciau.2c00047
ACS Meas. Sci. Au 2023, 3, 10−20

EXPERIMENTAL SECTION

Materials and Equipment

ANT, MBA, DBA, TET, FLR, EOY, and ERY were all obtained from Sigma-Aldrich (St. Louis, MO). Polystyrene (PS) beads for preparing ANT and DBA dispersed in a solid matrix were also obtained from Sigma-Aldrich (St. Louis, MO). Toluene was obtained from Fischer Scientific (Fairlawn, NJ) with a purity >99.5%. Unless specified otherwise, all data were acquired with PAH dissolved in toluene or xanthene dyes in water. Quartz cuvettes used for UV−vis and fluorescence measurements are from Raminescent LLC. Fluorescence measurements were performed with a Horiba Fluoromax-4 spectrofluorometer (Edison, NJ) equipped with a TC1 Quantum Northwest temperature controller together with a Koolance EXT-440 liquid cooling system. UV−vis spectra were obtained using a Shimadzu UV-2600i spectrophotometer equipped with a CPS-100 temperature controller (Duisburg, Germany). The accuracy of these temperatures is ±0.1 °C.

PAH in Solidified Polystyrene

Solidified gel solutions were prepared by first dissolving near-saturated polystyrene beads in toluene. 35 μL of 0.5 mM PAHs in toluene was added to 4.0 mL of PS solution. The sample was then stirred with a cleaned syringe for 5 min. The sample was left to settle for 1 day and then poured directly into a quartz cuvette. After 1 h of equilibrium time, the sample was then dried in a Fischer Scientific Isotemp oven at 75 °C for 21 h. The samples were then ready for analysis once the sample was cooled to room temperature. The PAH concentration in the dried PS matrix is about 10 μM, which was estimated based on the volume of solidified PS.

UV−Vis Spectrophotometric Acquisition

UV−vis spectra were acquired in 10 °C increments from 20 to 60 °C for the PAHs, and in 15 °C increments from 20 to 65 °C for the xanthene dyes. For each temperature-dependent UV−vis spectral acquisition, an equilibrium time of 10 min was given after the temperature controller reached the preselected temperature to ensure the sample inside the cuvette achieved the temperature shown in the temperature controller. This equilibrium time was determined based on the fluorescence thermometric method developed in this work (*vide infra*). The slit-width was set to 2 nm at a medium scanning speed.

TPL Spectral Acquisition

The TPL spectra were acquired with the excitation wavelengths indicated in the fluorescence excitation spectra and with the emission wavelengths indicated in the fluorescence emission spectra shown in Figure 1. For the TPL measurement at each specified temperature, an equilibrium time of 10 min was given after the temperature controller reached the preselected temperature to ensure the sample inside the cuvette achieved the temperature shown in the temperature controller. The slit-widths of the excitation and emission monochromators were both set to 2 nm. The integration time for each data point is 0.3 s. Unless specified otherwise, all data shown in this work are acquired with PAH dissolved in toluene and xanthene dyes in water.

Ratiometric Fluorescence Thermometry

A mixture of ANT and DBA was prepared, and the fluorescence emission spectra of the mixture were obtained with a 5 °C increment from 20 to 65 °C. The excitation wavelength for these emission spectra is chosen so that the difference in the temperature dependence of the ANT and DBA fluorescence is maximized. The temperature-dependent fluorescence spectra were obtained over four cycles (up−down−up−down) with the same samples to examine the method reproducibility.

Data Analysis

The TPL data allow visualization and quantification of emission intensity changes as a function of the sample temperature, excitation wavelength, and emission wavelengths. However, to probe the temperature effects on the fluorophore quantum yield (QY), one must also take into consideration the temperature effects on the fluorophore light absorption because fluorescence intensity is a function of the fluorophore light absorption and QY, as depicted by a recently developed first-principle model (eq 1). It is emphasized that this model is applicable only for the simplest cases where the fluorophore is the only light absorber and emitter, as are samples used in this work.

$$I(\lambda_x, \lambda_m, T) = I(\lambda_x)\, R(\lambda_m, T) A_{x,f} Q(\lambda_x, \lambda_m, T) 10^{-A_{x,f}d_x - A_{m,f}d_m} \quad (1)$$

$I(\lambda_x)$ represents the excitation power, $R(\lambda_m, T)$ is the detection responsivity, and $Q(\lambda_x, \lambda_m, T)$ indicates the fluorescence quantum yield. $A_{x,f}$ and $A_{m,f}$ are the UV−vis absorbances of the PL molecules at their excitation and emission wavelength, respectively. For small-molecular fluorophores dissolved in solution, their UV−vis spectra can be approximated as their absorbance spectra. In this case, $A_{x,f}$ and $A_{m,f}$ are the UV−vis intensities at the excitation and emission wavelength, respectively. d_x and d_m are the effective excitation and detection path length in cm. The exponent term in eq 1 depicts the sample inner filter effect (IFE) imposed by the sample absorption at excitation and emission wavelengths. The values of d_x and d_m can be readily quantified experimentally using a solvent-Raman spectroscopic method.[52] T represents the stimuli treatment of interest, which is the temperature effect for this work.

The combined UV−vis and TPL measurements enabled experimental quantification of the IFE-corrected fluorophore fluorescence (eq 2), temperature effects on the wavelength-specific fluorescence QY (eq 3), and temperature effects on the integrated fluorescence QY (eq 4). T_s and T_r refer to the sample and reference temperature, respectively. The ratios on the left-hand side of eqs 3 and 4 are referred to as the ratiometric wavelength-specific QY (rWSQY) and the ratiometric total fluorescence QY (rTQY), respectively. The detailed derivation of eqs 1−4 has been shown in an earlier report.[39]

$$I^{corr}(\lambda_x, \lambda_m, T) = I(\lambda_x, \lambda_m, T) 10^{A_{x,f}d_x + A_{m,f}d_m} \quad (2)$$

$$\frac{Q(\lambda_x, \lambda_m, T_s)}{Q(\lambda_x, \lambda_m, T_r)} = \frac{I^{corr}(\lambda_x, \lambda_m, T_s)}{I^{corr}(\lambda_x, \lambda_m, T_{20})} \frac{A_{x,f}(T_r)}{A_{x,f}(T_s)} \quad (3)$$

$$\frac{Q_t(\lambda_x, T_s)}{Q_t(\lambda_x, T_r)} = \frac{\int_{\lambda_1}^{\lambda_2} I^{corr}(\lambda_x, \lambda_m, T_s)\, d\lambda_m}{\int_{\lambda_1}^{\lambda_2} I^{corr}(\lambda_x, \lambda_m, T_{20})\, d\lambda_m} \frac{A(\lambda_x, T_r)}{A(\lambda_x, T_s)} \quad (4)$$

RESULTS AND DISCUSSION

Temperature Effects on the PAH Fluorescence

Temperature-dependent TPL spectral acquisition is a relatively lengthy process. To ensure the integrity of experimental data for probing the temperature effects, it is imperative to confirm fluorophore photostability during the spectral acquisition. Depending on the range of excitation, detection wavelength range, and spectral resolution, one set of TPL spectra at one specific temperature can take up to 30 min. In this case, a complete set of TPL data comprising five temperature points requires 2.5 h of continuous light illumination on the fluorescent samples, which can be too long for fluorophores with relatively poor photostability. PAHs are highly stable during all of the temperature-dependent TPL measurements, with excitation wavelength varying from 300 nm all the way to their red absorption edge (Figure 1). However, significant photobleaching occurs if the excitation wavelength begins at 300 nm for the xanthene dyes and with five temperature points (Figure S1). To ensure the integrity of the data for studying the temperature effect, xanthene TPL measurements are acquired in a relatively narrow range, as indicated in Figure

https://doi.org/10.1021/acsmeasuresciau.2c00047
ACS Meas. Sci. Au 2023, 3, 10−20

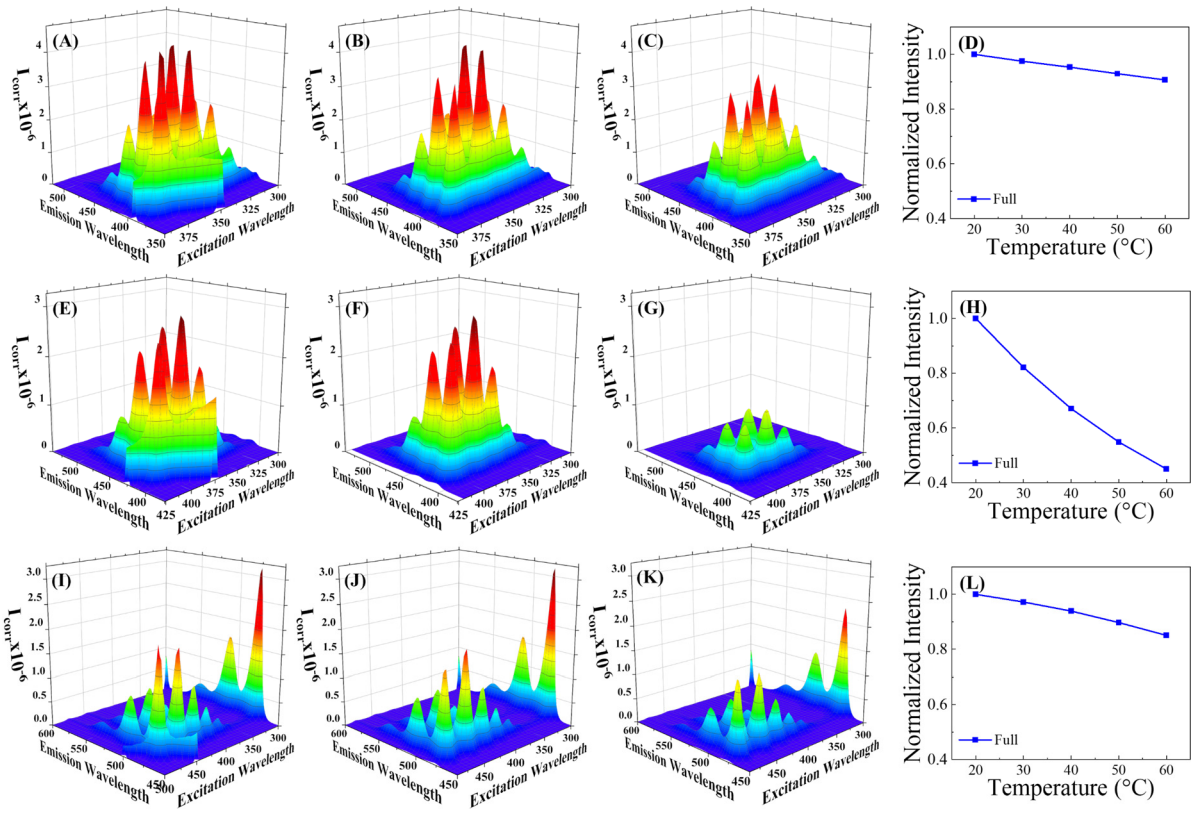

Figure 2. (first column) As-acquired and (second and third columns) scattering-removed TPL spectra obtained for (first row) ANT, (second row) DBA, and (third row) TET. The data shown in the first and second columns are acquired with a sample at 20 °C, while those in the third column are acquired at 60 °C. The fourth column shows the integrated fluorescence TPL intensity as a function of the sample temperature. The intensity normalization is obtained by using the data obtained at 20 °C as the reference.

1, and with only four temperature points (20, 35, 50, and 65 °C). The photostability of the PAHs and xanthene fluorophores under the experimental conditions is shown in the Supporting Information (Figures S2 and S3).

The as-acquired and the scatter-removed three-dimensional PAH TPL data (1st columns in Figure 2, and Figures S4–S6) are highly complicated. The spectra obtained with excitation wavelength within the shaded area in Figure 1 simultaneously contain ASSF, ORF, SSF, and light scattering features (Figure S7). Removal of the light scattering peak from the TPL spectra was performed using a local data replacement method (Supporting Information) that assumes that the fluorescence features excited with similar excitation wavelengths have the same shape. The effectiveness of the scattering peak removal method is graphically shown in Figure S7 which showed that the light scattering peak removal introduced no distortion in the fluorescence spectrum.

Both the 3D plots of the scattering-removed TPL data and the integrated TPL intensity showed that the temperature effects on PAH fluorescence depend critically on the PAH structure. As an example, the integrated total TPL intensity reduces by less than 10% and 12% for ANT and TET, respectively, when the sample temperature is increased from 20 to 60 °C. In contrast, DBA fluorescence reduced by nearly 55% across the same temperature range.

While the complete TPL plot is useful for its insights into the overall temperature effects on the fluorophore fluorescence, it is difficult to discern the possible difference in the temperature effects on SSF and ASSF. To resolve this issue, we divided the 3D TPL into 3D SSF and ASSF (Figure 3 and Figures S8–S10). Evidently, the temperature effects on the SSF and ASSF signals for each of the three PAH fluorophores all differ significantly. While the integrated SSF intensity monotonically decreases with increasing temperature, the integrated ASSF intensity can both increase and decrease with increasing sample temperatures in the probed temperature range. More specifically, the integrated ANT ASSF region increased by 10% when the sample temperature increased from 20 to 60 °C, while that for TET had no meaningful change (<5%). In contrast, the integrated DBA ASSF decreases by about ∼46% in this temperature range, which is smaller than the ∼56% intensity reduction observed with integrated SSF.

The difference in the temperature dependence between the integrated ASSF and SSF is consistent with the hot molecule hypothesis for the ASSF emission.[42] Hot molecules refer to the fluorophores that are at ground electronic states but are at excited rotational and vibrational states. Raising temperatures have two effects on ASSF. On one hand, they enhance the population of hot molecules according to the Boltzmann's distribution law, which is beneficial for increasing the ASSF intensity. On the other hand, increasing the sample temperature can change the relative rates between the radiative and nonradiative decays of the excited molecules, which can lead to enhanced or reduced ASSF intensity. Since the latter mechanism is in play for the temperature effects on both SSF and ASSF, it is reasonable to expect that raising the temperature has a less negative impact on ASSF than on SSF. This conclusion is further supported by the xanthene fluorophores (*vide infra*).

https://doi.org/10.1021/acsmeasuresciau.2c00047
ACS Meas. Sci. Au 2023, 3, 10–20

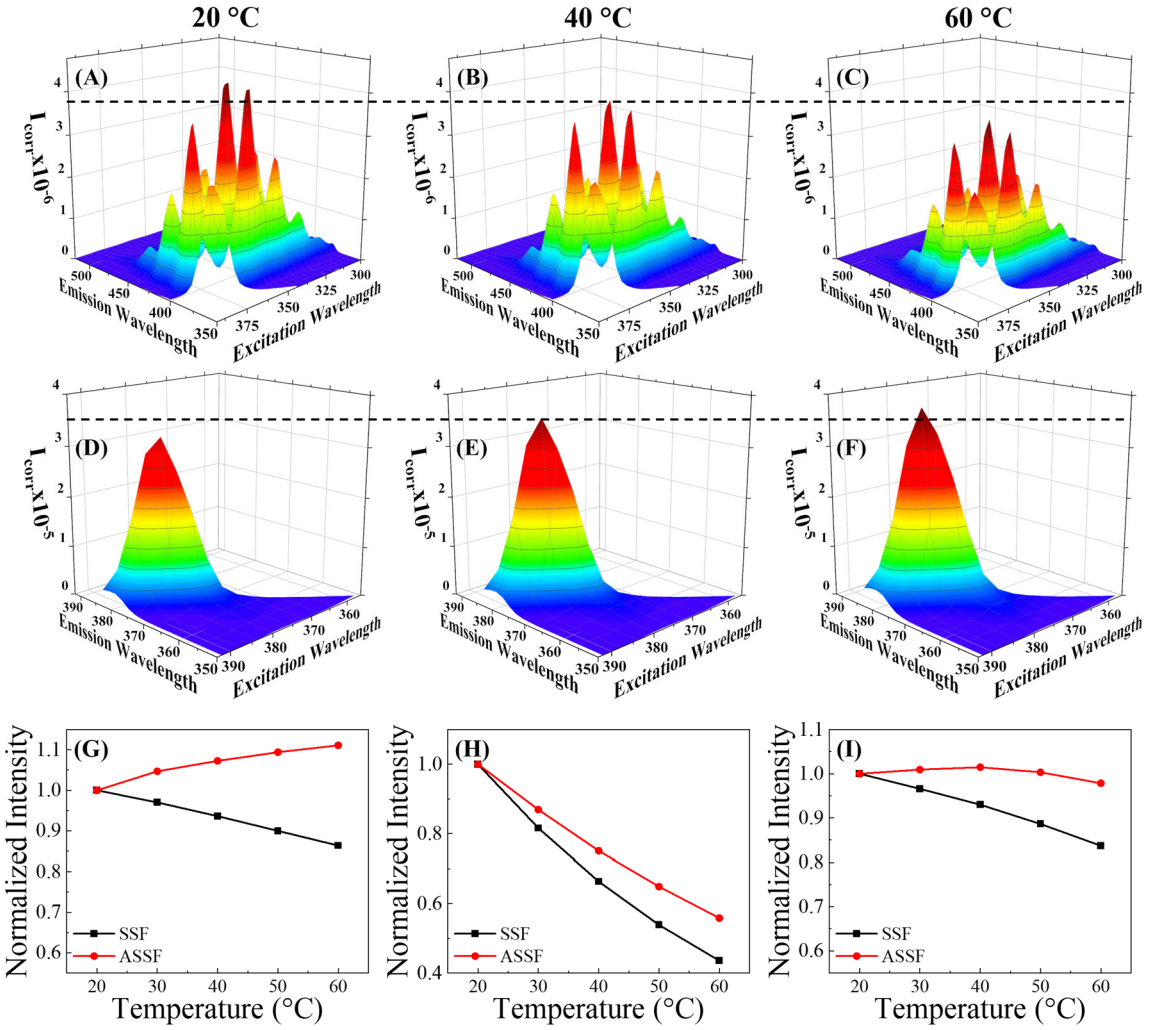

Figure 3. (A–C) 3D plots of the ANT SSF at 20, 40, and 60 °C, respectively. (D–F) 3D plots of the ANT ASSF at 20, 40, and 60 °C, respectively. (G–I) Normalized total SSF and ASSF intensities as a function of the sample temperature of ANT, DBT, and TET. The intensity normalization is obtained by using the data obtained at 20 °C as the reference.

TPL provided a convenient way for examining the possible wavelength dependence of the temperature effects on fluorophore fluorescence. A side-by-side comparison of the fluorescence excitation spectra monitored with two different emission wavelengths (Figure 4, first and second columns) and the fluorescence emission spectra excited with two different excitation wavelengths (Figure 4, third and fourth columns) showed that the temperature effects on ANT (Figure 4A–D), DBA (Figure 4E–H), and TET (Figure 4I–L) fluorescence depend on both the excitation and emission wavelengths. As an example, the relative fluorescence intensity changes in the excitation spectra shown in the first column are much smaller than those shown in the second column. Conversely, a similar difference exists between the data shown in the third and fourth columns.

A heat plot is an efficient and concise way for visualizing the global excitation and emission wavelength dependence of the temperature effects on the fluorophore fluorescence (Figure 5 and Figure S11). Depending on specific excitation and emission wavelengths, both normal or reversed temperature effects have been observed on ANT (Figure 5A) and TET (Figure 5C) fluorescence. The normal temperature effect refers to a fluorescence intensity decrease with increasing sample temperature, while the reversed temperature effect represents increased fluorescence intensity with increasing temperature. Even though raising the temperature invariably reduces the DBA fluorescence, the degree of the fluorescence intensity reduction depends on the specific excitation and emission wavelengths (Figure 5B).

The excitation and emission wavelength dependence are also evident in the normalized integrated emission spectra (Figure 5D–F) and the normalized integrated excitation spectra (Figure S12). These data are taken by spectral integration by a simple summation of the emission or excitation intensity over the entire excitation or emission wavelength range, while normalization is performed by dividing the integrated fluorescence emission intensity obtained at the temperature of interest by that obtained at 20 °C. The sensitivity of the integrated fluorescence emission intensity depends critically on the excitation wavelengths (Figure 5D–F).

Empirically, the sensitivity of integrated fluorescence intensity correlates strongly with the PAH UV–vis absorbance spectra. The integrated fluorescence excited with wavelengths corresponding to red shoulder wavelengths in the vibrationally resolved PAH UV–vis absorbance peaks is much more sensitive to temperature change than that excited at the blue

https://doi.org/10.1021/acsmeasuresciau.2c00047
ACS Meas. Sci. Au 2023, 3, 10–20

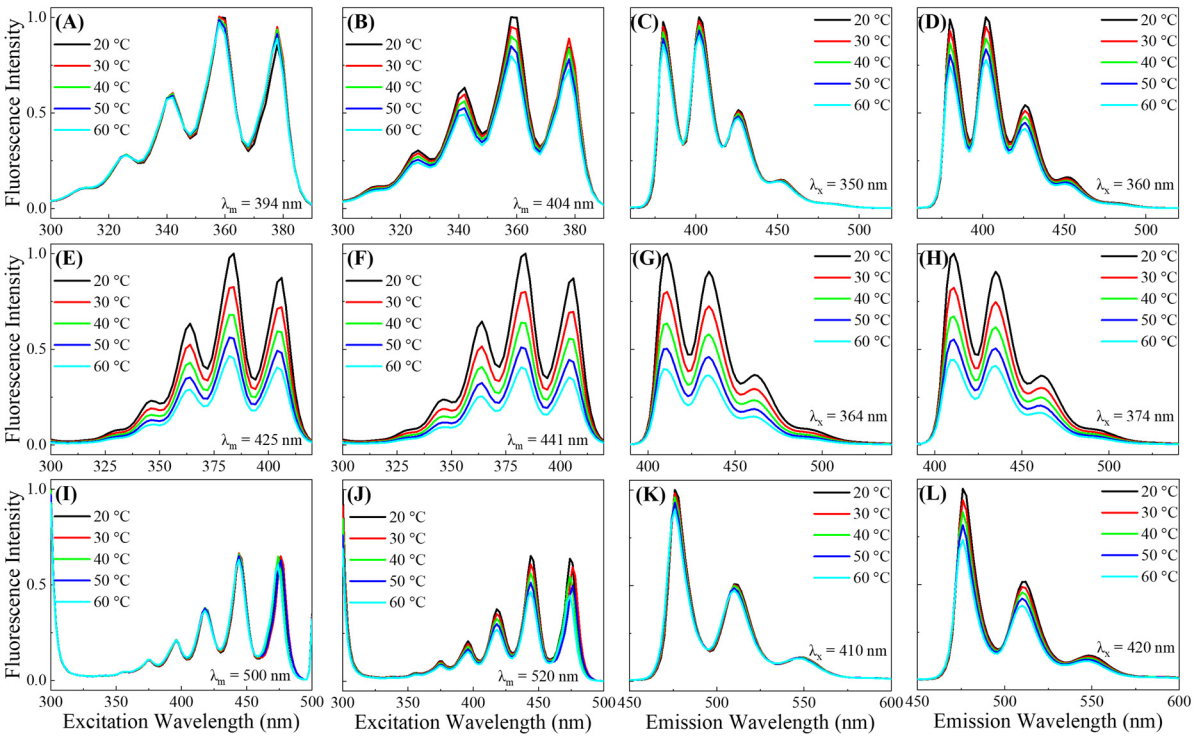

Figure 4. Representative temperature-dependent fluorescence (first and second columns) excitation spectra and (third and fourth columns) emission spectra of (first row) ANT, (second row) DBA, and (third row) TET. The emission and excitation wavelengths used for the spectral acquisition are shown in the plots.

shoulder wavelengths (Figure 5G–I). These red and blue shoulder wavelengths are highlighted with red and blue dashed lines in Figure 5.

The combined temperature-dependent UV–vis absorbance and TPL study enables us to quantify the PAH rWSQY (Figure 5J–L and Figure S13) and rTQY as a function of the excitation wavelengths (Figure 5M–O). rWSQY and rTQY values are evaluated using eqs 3 and 4, respectively. The heat plot of rWSQY data showed that the temperature effects on the PAH QY are both excitation- and emission-wavelength-dependent. The general patterns of the rWSQY heat plots (Figure 5J–L) are very similar to the heat plots of the normalized fluorescence intensity (Figure 5A–C). However, rTQY spectra (Figure 5M–O) are approximately independent of the excitation wavelength, which is in sharp contrast to relatively strong excitation wavelength dependence in the normalized integrated emission intensity (Figure 5D–F). These results indicate that the differences seen in the integrated fluorescence intensities among different excitation wavelengths are due predominantly to the temperature effects on the PAH UV–vis absorbance but not to those on the integrated emission QY.

Consistent with earlier reports, the temperature effects on DBA fluorescence are much stronger than those on ANT and TET.[53−55] The high sensitivity of DBA fluorescence to sample temperature has been attributed to the heavy-atom effect, a theory commonly used to explain the low QY of fluorophores with heavy atoms. It has been assumed that, at elevated temperatures, fluorophores with heavy atoms become more prone to nonradiative decay, resulting in reduced fluorescence emission. This hypothesis is consistent with our observation that the fluorescence of monobrominated anthracene has a temperature sensitivity higher than that of ANT but lower than that of DBA (Figure S14).

Temperature Effects on Xanthene Fluorescence

FLR, EOY, and ERY serve as an excellent set of fluorophores for further testing the significance of the heavy-atom effect in governing the temperature effects of fluorophore fluorescence because the only difference in these fluorophores is the number and type of heavy atoms. FLR has no heavy atoms, while EOY and ERY are two FLR derivatives containing four bromine and iodine substituents, respectively, at the same substitution positions. All xanthene dyes exhibit a strongly temperature-dependent ASSF when excited at the wavelength region where their UV–vis absorption and emission spectra overlap (Figures S15–S17), which is similar to what has been observed with PAH dyes. Surprisingly, however, the temperature effects on FLR (Figure 6A–D), EOY (Figure 6E–H), and ERY (Figure 6I–L) are contradictory to what one would expect from the heavy-atom effects (Figure 6 and Figures S18–S20). FLR has no heavy atoms but has the largest decrease with increasing sample temperature, while the peak intensity of EOY has no significant temperature dependence. ERY, the xanthene dye with iodine substitutions, exhibits reversed temperature effects at its peak emission. These data argue strongly against the possibility of the heavy-atom effect as a dominant mechanism for the temperature effects on fluorophore fluorescence. Otherwise, one would expect ERY to have the most significant intensity reduction, followed by EOY, and then FLR with increasing sample temperature. The detailed reason for this effect is currently unclear. Nonetheless, the data obtained with FLR, EOY, and ERY showed that the heavy-atom effect is unlikely a universal mechanism for the temperature effect on fluorophore fluorescence.

https://doi.org/10.1021/acsmeasuresciau.2c00047
ACS Meas. Sci. Au 2023, 3, 10–20

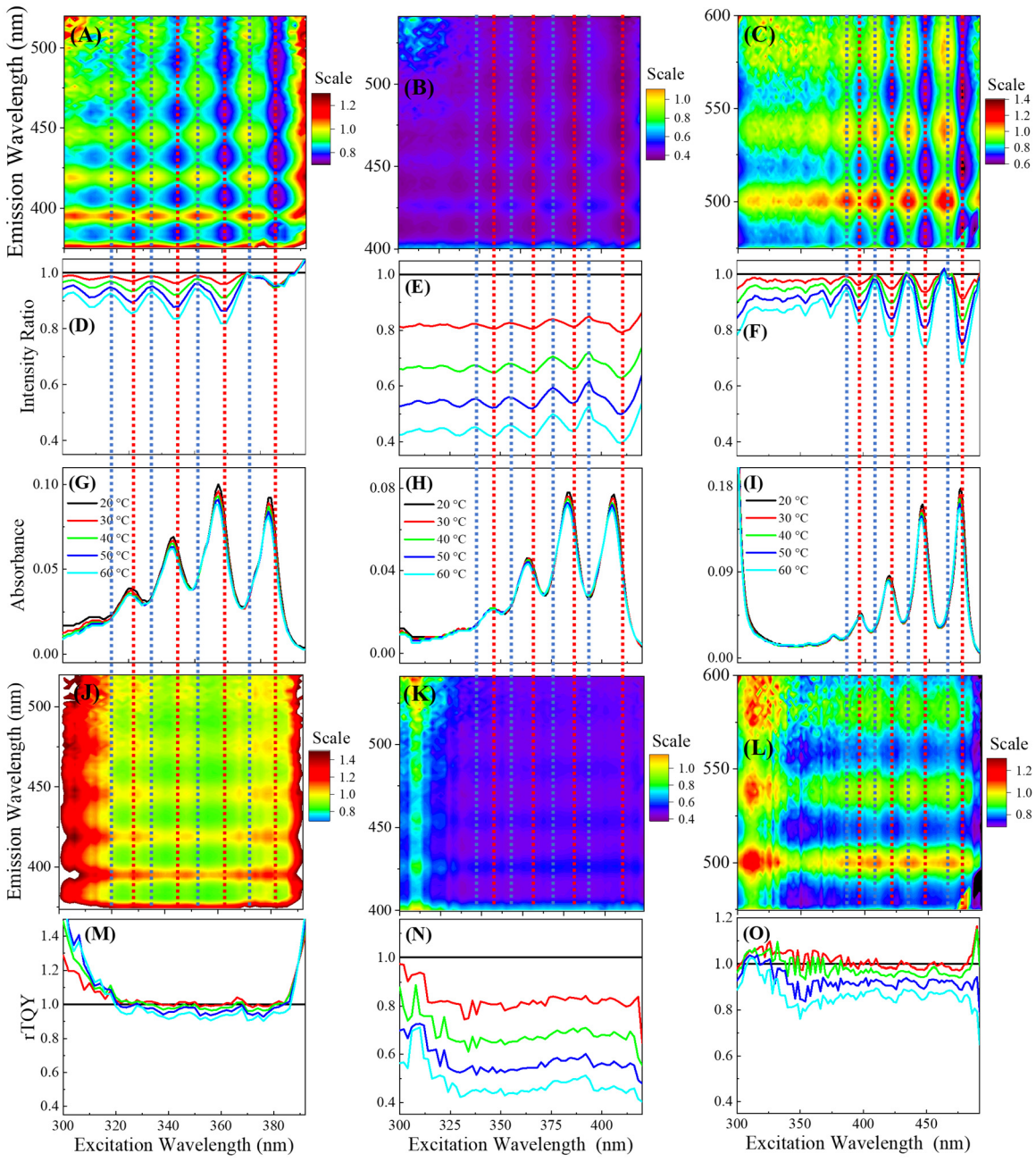

Figure 5. (first row) Example heat plots of fluorescence intensity ratios (60 °C/20 °C). (second row) Normalized temperature-dependent integrated fluorescence intensity spectra. (third row) Temperature-dependent UV−vis absorbance spectrum. (fourth row) Example heat plots of the rWSQY at T = 60 °C. (fifth row) Temperature-dependent rTQY spectra of (first column) ANT, (second column) DBA, and (third column) TET. Yellow, orange to maroon, and green to purple in the heat plots depict values of 1, higher than 1, and less than 1, respectively. The vertical blue and red dashed lines correspond to red and blue peak shoulder wavelengths in the UV−vis absorbance spectra.

Consistent with what is observed with the PAH dyes, the temperature effects of the xanthene ASSF and SSF are also very different (Figures S15−S17). Their integrated ASSFs all exhibit reversed temperature effects, i.e., increasing ASSF intensity with increase temperature. ERY exhibits the largest ASSF intensity increase, followed by EOY, and FLR, which again is opposite the expected trend. Also in contrast to that trend, the integrated FLR SSF exhibits no significant temperature dependence, while those for both ERY and EOY show reverse temperature effects as compared to their respective ASSF counterparts.

Impact of Sample Matrix on the Temperature Effects on PAH Fluorescence

Dynamic quenching due to the enhanced solvent/fluorophore interactions (exciplex formation and dynamic quenching) at an elevated temperature was also proposed as a mechanism for the reduced fluorescence emission at high sample temperature. To test this hypothesis, we compared the temperature dependence of the fluorescence intensity of PAHs dispersed in toluene solution to the same PAHs dispersed in a solidified polystyrene matrix. Surprisingly, the degree of the temperature dependence of the PAH in liquid is very similar to that in a solid (Figure S21). These data strongly suggest that the

https://doi.org/10.1021/acsmeasuresciau.2c00047
ACS Meas. Sci. Au 2023, 3, 10−20

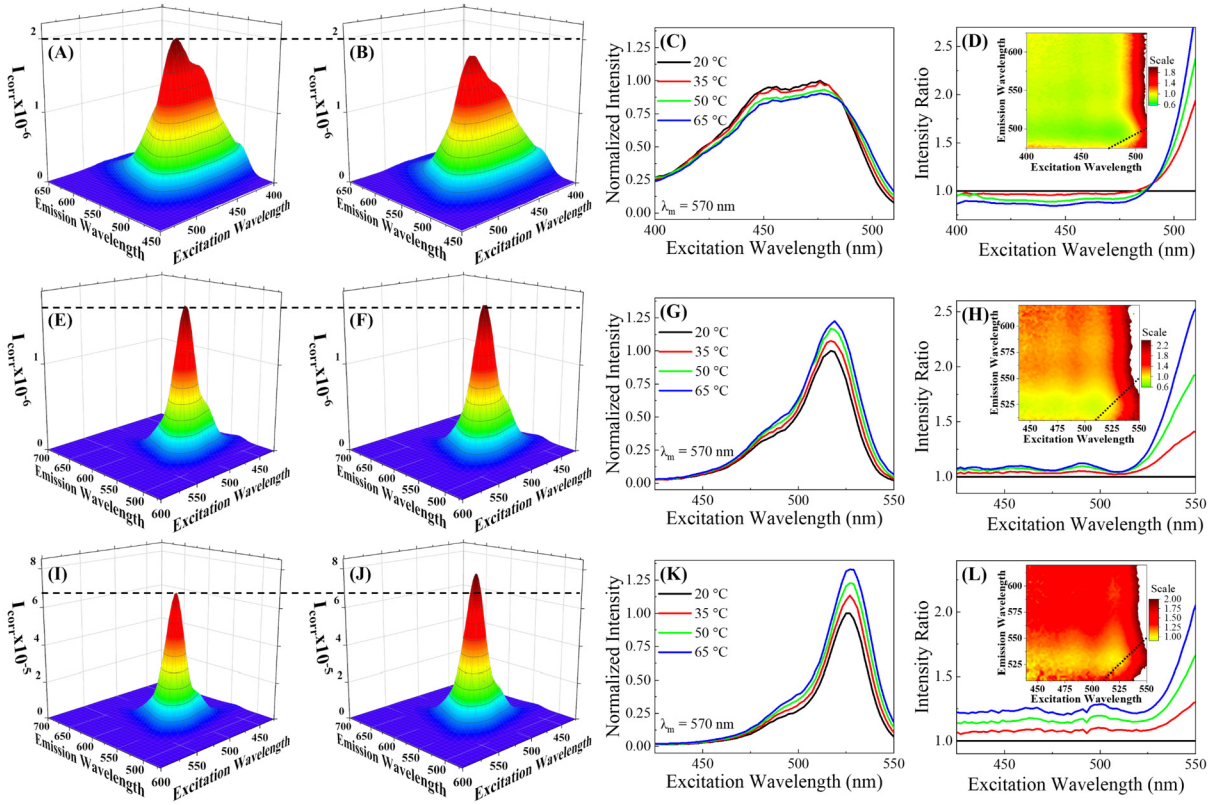

Figure 6. (first column) TPL 20 °C, (second column) TPL 65 °C, and (third column) representative temperature dependence fluorescence excitation spectra. (fourth column) Integrated intensity as a function of temperature of (first row) FLR, (second row) EOY, and (third row) ERY. The insets in the fourth column are the heat maps depicting the TPL intensity ratio of 65 and 20 °C.

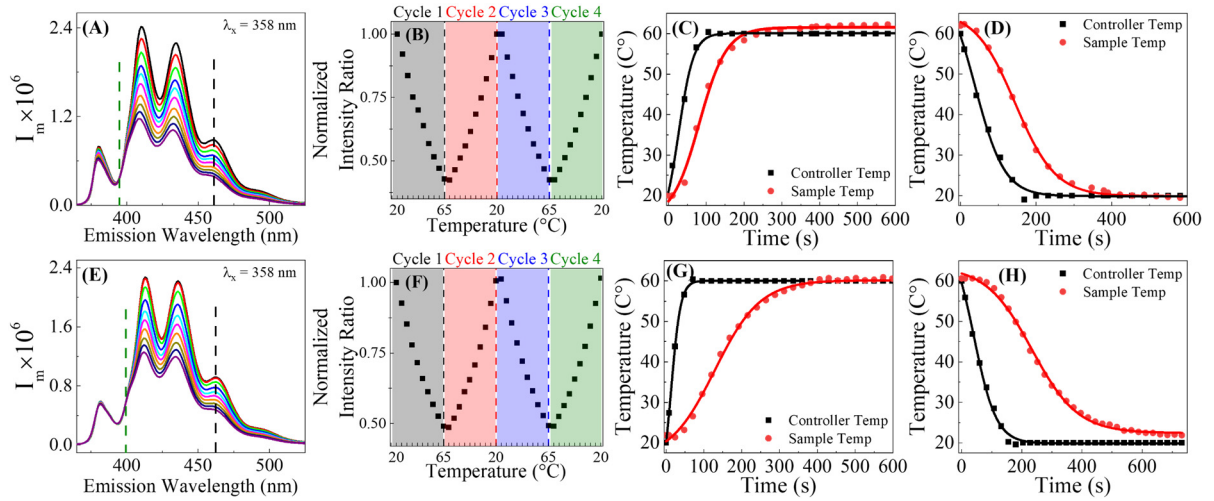

Figure 7. (first column) Fluorescence emission from 20 to 65 °C. (second column) Peak intensity of four cycles. (third and fourth columns) Temperature of controller versus sample temperature when heating and cooling, respectively, for (first row) the solution and (second row) the solid ANT/DBA mixture in toluene. Black dots in panels C, D, G, and H represent the temperature shown at the temperature controller, while the red dots are the measured temperatures based on the fluorescence intensity ratios.

dynamic quenching by solvent/fluorophore interaction is unlikely a main contributor to the PAH signal reduction at elevated temperatures. Otherwise, one would expect smaller temperature effects on the PAHs dispersed in a solid than those dissolved in liquid.

Ratiometric Fluorescence Thermometry

The preceding sections showed that TPL measurements are extraordinarily informative in providing insights that have not been accessible before for a fundamental understanding of the temperature effects on fluorophore optical properties. The learning from the TPL data is also important for rational measurement design for applications where the fluorophore temperature sensitivity is of concern. As an example, based on TPL data obtained with the PAHs, we designed a ratiometric fluorescence thermometric method for *in situ* real-time measurements of the actual sample temperatures inside

https://doi.org/10.1021/acsmeasuresciau.2c00047
ACS Meas. Sci. Au 2023, 3, 10−20

fluorescence cuvettes placed in a temperature-controlled sample holder. Such measurements are critical for analytical and physical chemistry research because temperature-dependent spectroscopic study has become increasing popular, but monitoring the difference between the controller's temperature and actual sample temperature is difficult.

Since DBA fluorescence is sensitive to sample temperatures, and ANT fluorescence is highly robust against the temperature variation, their mixture allows us to develop a ratiometric fluorescence thermometric method for quantification of the sample temperature. The selection of the excitation wavelength is guided by the following criteria: (1) both ANT and DBA are fluorescence active at the excitation wavelength, and (2) the temperature effects under the excitation wavelength are high for DBA but negligibly small for ANT emission. For the selection of the two emission wavelengths for the ratiometric fluorescence thermometric method, the reference emission should have negligible temperature sensitivity, while the sampling peak should have maximum temperature sensitivity.

The effectiveness of this ratiometric fluorometric strategy is demonstrated by the data shown in Figure 7. Under excitation at 358 nm, both ANT and DBA are fluorescence active (Figure 7A,E). The emission near the 400 nm region is chosen as the reference because the fluorescence at this wavelength is essentially independent of the sample temperature. The fluorescence emissions at wavelengths above 420 nm are all sensitive to the sample temperature variations. The fluorescence intensity ratio between the selected emission wavelengths correlates strongly with the sample temperatures (Figure 7B,F). Such a correlation is highly reproducible for the four cycles of the temperature ramping up and down measurement, showing the robustness of this ratiometric method.

There are significant lag times between the controller temperature and the actual sample temperature to reach the targeted temperatures during both the sample heating and cooling processes. The lag time is longer for the solidified sample (Figure 7E−H) than for the solution sample (Figure 7A−D) and longer for the sample cooling (Figure 7D,H) than for the sample heating. For example, it took 50 s longer for the solution sample temperature to reach a preset heating temperature indicated by the temperature controller, which is in comparison to the 300 s lagging time observed for the solid sample. The lag time for the solution sample and the temperature to reach the preset cooling temperature is about 200 s, while that for the solid sample is about 600 s. This *in situ*, real-time determination of the measurement lagging time is important for improving the reliability of temperature-dependent spectroscopic measurements. Guided by these findings, the temperature-dependent TPL measurements presented in this work are all acquired after the temperature controller has maintained the preset temperature for 10 min to ensure that the samples actually reach the temperature shown on the temperature controller.

CONCLUSION

We presented a temperature-dependent total photoluminescence spectroscopic technique, including measurement procedures, as well as highlighted the data analysis and visualization methodologies. When used in combination with the temperature-dependent UV−vis absorbance measurements, the TPL method introduced in this work offered a series of insights that have not been available before. The key novel insights enabled by this new measurement strategy include the following: (1) The temperature-induced fluorescence intensity change can be due to the temperature effects on the fluorophore QY and/or its UV−vis absorbance. Therefore, a combination of UV−vis absorbance and fluorescence study is necessary for one to derive a mechanistic understanding of the temperature effects on the fluorophore fluorescence. (2) The heavy atom substitution in the xanthene dyes has no significant impact on the temperature-dependent fluorescence, excluding the possibility that the heavy-atom effect proposed for the large temperature dependence of the brominated anthracene is a universal mechanism governing the temperature effects on fluorophore fluorescence. (3) The temperature effects on the fluorophore fluorescence observed with all model fluorophores are strongly wavelength-dependent, which highlights the importance of the TPL methodology presented in this work. For applications where the temperature effects on materials fluorescence are important, it is advised to perform a temperature-dependent TPL study to optimize the measurement design. The insight from such measurements is important not only for a fundamental understanding of materials optical processes but also for rational measurement design in applications that require a maximum or minimum temperature sensitivity. The example ratiometric fluorescence thermometry design could lay the foundation for future development of nanoscale temperature sensors by fabricating fluorescence nanoparticles comprising temperature-sensitive and temperature-insensitive dyes. We believe the measurement technique as well as the data process, analysis, and visualization methods presented in this work will be adopted broadly by physical, analytical, and material chemists for characterizations and applications of photoluminescence materials.

ASSOCIATED CONTENT

Supporting Information

The Supporting Information is available free of charge at https://pubs.acs.org/doi/10.1021/acsmeasuresciau.2c00047.

Complete 3D TPL, ASSF, and SSF data of PAH and xanthene dyes; scattering removal method and validation; comparison of the temperature effects on PAH in solution and a solidified polystyrene matrix; and comparison of the temperature effects on ANTs with different bromine substitution (PDF)

AUTHOR INFORMATION

Corresponding Author

Dongmao Zhang − *Department of Chemistry, Mississippi University, Mississippi State, Mississippi 39759, United States;* orcid.org/0000-0002-2303-7338; Phone: (662)-325-6752; Email: dongmao@chemistry.msstate.edu

Authors

Max Wamsley − *Department of Chemistry, Mississippi University, Mississippi State, Mississippi 39759, United States;* orcid.org/0000-0001-6790-4846

Weiyu Peng − *Department of Chemistry, Mississippi University, Mississippi State, Mississippi 39759, United States*

Weinan Tan − *Department of Chemistry, Mississippi University, Mississippi State, Mississippi 39759, United States*

Pathum Wathudura − *Department of Chemistry, Mississippi University, Mississippi State, Mississippi 39759, United States*

Xin Cui − *Department of Chemistry, Mississippi University, Mississippi State, Mississippi 39759, United States;* orcid.org/0000-0001-8689-7100

Shengli Zou − *Department of Chemistry, University of Central Florida, Orlando, Florida 32816, United States;* orcid.org/0000-0003-1302-133X

Complete contact information is available at: https://pubs.acs.org/10.1021/acsmeasuresciau.2c00047

Author Contributions

CRediT: **Max Wamsley** data curation (equal), formal analysis (equal), investigation (equal), methodology (equal), validation (equal), visualization (equal), writing-original draft (equal), writing-review & editing (equal); **Weiyu Peng** data curation (equal); **Weinan Tan** data curation (equal), resources (equal); **Dongmao Zhang** conceptualization (lead), formal analysis (lead), funding acquisition (lead), investigation (equal), methodology (equal), project administration (lead), resources (lead), supervision (lead), validation (lead), visualization (lead), writing-original draft (lead), writing-review & editing (lead).

Notes

The authors declare no competing financial interest.

■ ACKNOWLEDGMENTS

This work was supported in part by the Center of Biomedical Research Excellence Program funded through the Center for Research Capacity Building (CRCB) in the National Institute for General Medical Sciences (Grant P20GM103646) and by NSF CHE 2203571. The content is solely the responsibility of the authors and does not necessarily represent the official views of the National Institutes of Health or National Science Foundation.

■ REFERENCES

(1) Budden, P. J.; et al. Singlet Exciton Fission in a Modified Acene with Improved Stability and High Photoluminescence Yield. *Nat. Commun.* **2021**, *12*, 1527.

(2) Liu, W.; Zhu, K.; Teat, S. J.; Dey, G.; Shen, Z.; Wang, L.; O'Carroll, D. M.; Li, J. All-in-One: Achieving Robust, Strongly Luminescent and Highly Dispersible Hybrid Materials by Combining Ionic and Coordinate Bonds in Molecular Crystals. *JACS.* **2017**, *139*, 9281−9290.

(3) Zhu, L.; Zhang, J.; Guo, Y.; Yang, C.; Yi, Y.; Wei, Z. Small Exciton Binding Energies Enabling Direct Charge Photogeneration Towards Low-Driving-Force Organic Solar Cells. *Angew. Chem., Int. Ed.* **2021**, *60*, 15348−15353.

(4) Wang, Q.; et al. Efficient Sky-Blue Perovskite Light-Emitting Diodes Via Photoluminescence Enhancement. *Nat. Commun.* **2019**, *10*, 5633.

(5) Nurhayati; Suendo, V.; Alni, A.; Nugroho, A. A.; Majima, Y.; Lee, S.; Nugraha, Y. P.; Uekusa, H. Revealing the Real Size of a Porphyrin Molecule with Quantum Confinement Probing Via Temperature-Dependent Photoluminescence Spectroscopy. *J. Phys. Chem. A* **2020**, *124*, 2672−2682.

(6) Sun, Q.; Wang, S.; Zhao, C.; Leng, J.; Tian, W.; Jin, S. Excitation-Dependent Emission Color Tuning from an Individual Mn-Doped Perovskite Microcrystal. *JACS.* **2019**, *141*, 20089−20096.

(7) Zeng, H.; Zhou, T.; Wang, L.; Xie, R.-J. Two-Site Occupation for Exploring Ultra-Broadband near-Infrared Phosphor—Double-Perovskite La2mgzro6:Cr3+. *Chem. Mater.* **2019**, *31*, 5245−5253.

(8) Okabe, K.; Inada, N.; Gota, C.; Harada, Y.; Funatsu, T.; Uchiyama, S. Intracellular Temperature Mapping with a Fluorescent Polymeric Thermometer and Fluorescence Lifetime Imaging Microscopy. *Nat. Commun.* **2012**, *3*, 705.

(9) Sun, Z.-B.; Liu, J.-K.; Yuan, D.-F.; Zhao, Z.-H.; Zhu, X.-Z.; Liu, D.-H.; Peng, Q.; Zhao, C.-H. 2,2′-Diamino-6,6′-Diboryl-1,1′-Binaphthyl: A Versatile Building Block for Temperature-Dependent Dual Fluorescence and Switchable Circularly Polarized Luminescence. *Angew. Chem., Int. Ed.* **2019**, *58*, 4840−4846.

(10) Ma, L.; Zhou, Y.; Zhang, Z.; Liu, Y.; Zhai, D.; Zhuang, H.; Li, Q.; Yuye, J.; Wu, C.; Chang, J. Multifunctional Bioactive Nd-Ca-Si Glasses for Fluorescence Thermometry, Photothermal Therapy, and Burn Tissue Repair. *Sci. Adv.* **2020**, *6*, eabb1311.

(11) Greiner, G. The Unusual Temperature Dependence of the Fluorescence Intensity and Lifetime of Anthracene in Ethanol. *J. Photochem. Photobiol.* **2000**, *137*, 1−7.

(12) Li, L.; Peng, M.; Viana, B.; Wang, J.; Lei, B.; Liu, Y.; Zhang, Q.; Qiu, J. Unusual Concentration Induced Antithermal Quenching of the Bi2+ Emission from Sr2p2o7:Bi2+. *Inorg. Chem.* **2015**, *54*, 6028−6034.

(13) Kole, A. K.; Kumbhakar, P.; Ganguly, T. Observations of Unusual Temperature Dependent Photoluminescence Anti-Quenching in Two-Dimensional Nanosheets of Zns/Zno Composites and Polarization Dependent Photoluminescence Enhancement in Fungi-Like Zno Nanostructures. *J. Appl. Phys.* **2014**, *115*, 224306.

(14) Chen, L.; Chen, X.; Ma, R.; Lin, K.; Li, Q.; Lang, J.-P.; Liu, C.; Kato, K.; Huang, L.; Xing, X. Thermal Enhancement of Luminescence for Negative Thermal Expansion in Molecular Materials. *JACS.* **2022**, *144*, 13688−13695.

(15) Franck, J.; Dymond, E. G. Elementary Processes of Photochemical Reactions. *J. Chem. Soc., Faraday Trans.* **1926**, *21*, 536−542.

(16) McClure, D. S. Triplet-Singlet Transitions in Organic Molecules. Lifetime Measurements of the Triplet State. *J. Chem. Phys.* **1949**, *17*, 905−913.

(17) Bowen, E. J.; Cook, R. J. 608. Temperature Coefficients of Fluorescence. *J. Chem. Soc.* **1953**, 3059−3061.

(18) Barradas, I.; Ferreira, J. A.; Thomaz, M. F. Intramolecular Heavy-Atom Effect and Intersystem-Crossing in Monohalogenated Pyrenes. *J. Chem. Soc., Faraday Trans. II.* **1973**, *69*, 388−394.

(19) Baba, M.; et al. Structure and Excited-State Dynamics of Anthracene: Ultrahigh-Resolution Spectroscopy and Theoretical Calculation. *J. Chem. Phys.* **2009**, *130*, 134315.

(20) Zhu, B.-S.; Li, H.-Z.; Ge, J.; Li, H.-D.; Yin, Y.-C.; Wang, K.-H.; Chen, C.; Yao, J.-S.; Zhang, Q.; Yao, H.-B. Room Temperature Precipitated Dual Phase Cspbbr3−Cspb2br5 Nanocrystals for Stable Perovskite Light Emitting Diodes. *Nanoscale.* **2018**, *10*, 19262−19271.

(21) Xu, L.; Li, Y.; Pan, Q.; Wang, D.; Li, S.; Wang, G.; Chen, Y.; Zhu, P.; Qin, W. Dual-Mode Light-Emitting Lanthanide Metal−Organic Frameworks with High Water and Thermal Stability and Their Application in White Leds. *ACS Appl. Mater. Interfaces.* **2020**, *12*, 18934−18943.

(22) Lu, T.; et al. Temperature-Dependent Photoluminescence in Light-Emitting Diodes. *Sci. Rep.* **2015**, *4*, 6131.

(23) Kwak, G.; Fukao, S.; Fujiki, M.; Sakaguchi, T.; Masuda, T. Temperature-Dependent, Static, and Dynamic Fluorescence Properties of Disubstituted Acetylene Polymer Films. *Che. Mater.* **2006**, *18*, 2081−2085.

(24) Peng, H.; Stich, M. I. J.; Yu, J.; Sun, L.-n.; Fischer, L. H.; Wolfbeis, O. S. Luminescent Europium(Iii) Nanoparticles for Sensing and Imaging of Temperature in the Physiological Range. *Adv. Mater.* **2010**, *22*, 716−719.

(25) Franklin, D.; Ueltschi, T.; Carlini, A.; Yao, S.; Reeder, J.; Richards, B.; Van Duyne, R. P.; Rogers, J. A. Bioresorbable Microdroplet Lasers as Injectable Systems for Transient Thermal Sensing and Modulation. *ACS Nano* **2021**, *15*, 2327−2339.

(26) Wang, J.-X.; Peng, L.-Y.; Liu, Z.-F.; Zhu, X.; Niu, L.-Y.; Cui, G.; Yang, Q.-Z. Tunable Fluorescence and Afterglow in Organic Crystals for Temperature Sensing. *J. Phys. Chem. Lett.* **2022**, *13*, 1985−1990.

(27) Cauzzi, D.; et al. Temperature-Dependent Fluorescence of Cu5Metal Clusters: A Molecular Thermometer. *Angew. Chem., Int. Ed.* **2012**, *51*, 9662−9665.
(28) Kaczmarek, A. M.; Suta, M.; Rijckaert, H.; Abalymov, A.; Van Driessche, I.; Skirtach, A. G.; Meijerink, A.; Van Der Voort, P. Visible and Nir Upconverting Er3+−Yb3+ Luminescent Nanorattles and Other Hybrid Pmo-Inorganic Structures for in Vivo Nanothermometry. *Adv. Funct. Mater.* **2020**, *30*, 2003101.
(29) Jang, C. H.; et al. Sky-Blue-Emissive Perovskite Light-Emitting Diodes: Crystal Growth and Interfacial Control Using Conjugated Polyelectrolytes as a Hole-Transporting Layer. *ACS Nano* **2020**, *14*, 13246−13255.
(30) Xue, J.; Noh, H. M.; Choi, B. C.; Park, S. H.; Kim, J. H.; Jeong, J. H.; Du, P. Dual-Functional of Non-Contact Thermometry and Field Emission Displays Via Efficient Bi3+ → Eu3+ Energy Transfer in Emitting-Color Tunable Gdnbo4 Phosphors. *Chem. Eng. J.* **2020**, *382*, 122861.
(31) Fang, M.-H.; Mahlik, S.; Lazarowska, A.; Grinberg, M.; Molokeev, M. S.; Sheu, H.-S.; Lee, J.-F.; Liu, R.-S. Structural Evolution and Effect of the Neighboring Cation on the Photoluminescence of Sr(Lial3)1−X(Simg3)Xn4:Eu2+ Phosphors. *Angew. Chem., Int. Ed.* **2019**, *58*, 7767−7772.
(32) Li, D.; et al. Thermally Activated Upconversion near-Infrared Photoluminescence from Carbon Dots Synthesized Via Microwave Assisted Exfoliation. *Small.* **2019**, *15*, 1905050.
(33) Buizza, L. R. V.; Wright, A. D.; Longo, G.; Sansom, H. C.; Xia, C. Q.; Rosseinsky, M. J.; Johnston, M. B.; Snaith, H. J.; Herz, L. M. Charge-Carrier Mobility and Localization in Semiconducting Cu2agbii6 for Photovoltaic Applications. *ACS. Energy. Lett.* **2021**, *6*, 1729−1739.
(34) Ware, W. R.; Baldwin, B. A. Effect of Temperature on Fluorescence Quantum Yields in Solution. *J. Chem. Phys.* **1965**, *43*, 1194−1197.
(35) Groot, M. L.; Peterman, E. J.; van Kan, P. J.; van Stokkum, I. H.; Dekker, J. P.; van Grondelle, R. Temperature-Dependent Triplet and Fluorescence Quantum Yields of the Photosystem Ii Reaction Center Described in a Thermodynamic Model. *Biophys. J.* **1994**, *67*, 318−330.
(36) Helenius, V.; Monshouwer, R.; van Grondelle, R. Temperature-Dependent Lifetimes and Quantum Yield of the Singlet and Triplet States of the B820 Subunit of Lhi Antenna Complex of Purple Bacterium Rhodospirillum Rubrum. *J. Phys. Chem. B* **1997**, *101*, 10554−10559.
(37) Blitz, M. A.; Heard, D. E.; Pilling, M. J.; Arnold, S. R.; Chipperfield, M. P. Pressure and Temperature-Dependent Quantum Yields for the Photodissociation of Acetone between 279 and 327.5 Nm. *Geophys. Res. Lett.* **2004**, *31*, L06111.
(38) Zhu, Y.; Kieber, D. J. Wavelength- and Temperature-Dependent Apparent Quantum Yields for Photochemical Production of Carbonyl Compounds in the North Pacific Ocean. *Environ. Sci. Technol.* **2018**, *52*, 1929−1939.
(39) Wamsley, M.; Nawalage, S.; Hu, J.; Collier, W. E.; Zhang, D. Back to the Drawing Board: A Unifying First-Principle Model for Correlating Sample Uv−Vis Absorption and Fluorescence Emission. *Anal. Chem.* **2022**, *94*, 7123−7131.
(40) Jablonski, A. Efficiency of Anti-Stokes Fluorescence in Dyes. *Nature.* **1933**, *131*, 839−840.
(41) Yan, L.; Li, B.; Song, Y.; Lv, Z.; Zheng, X.; Wu, Q.; Yang, Y. Optical Temperature Sensing Using the Multiphonon-Assisted Anti-Stokes-to-Stokes Fluorescence Intensity Ratio. *Opt. Lett.* **2017**, *42*, 3793−3795.
(42) Zhu, X.; Su, Q.; Feng, W.; Li, F. Anti-Stokes Shift Luminescent Materials for Bio-Applications. *Chem. Soc. Rev.* **2017**, *46*, 1025−1039.
(43) Wang, Z.; Zhao, J.; Di Donato, M.; Mazzone, G. Increasing the Anti-Stokes Shift in Tta Upconversion with Photosensitizers Showing Red-Shifted Spin-Allowed Charge Transfer Absorption but a Non-Compromised Triplet State Energy Level. *Chem. Commun.* **2019**, *55*, 1510−1513.
(44) Jollans, T.; Caldarola, M.; Sivan, Y.; Orrit, M. Effective Electron Temperature Measurement Using Time-Resolved Anti-Stokes Photoluminescence. *J. Phys. Chem. A* **2020**, *124*, 6968−6976.
(45) Zhou, J.; et al. Hot-Band Absorption of Indocyanine Green for Advanced Anti-Stokes Fluorescence Bioimaging. *Light. Sci. Appl.* **2021**, *10*, 182.
(46) Yeshchenko, O. A.; Dmitruk, I. M.; Dmytruk, A. M.; Alexeenko, A. A. Influence of Annealing Conditions on Size and Optical Properties of Copper Nanoparticles Embedded in Silica Matrix. *Mater. Sci. Eng. B* **2007**, *137*, 247−254.
(47) Biswas, S.; Kole, A. K.; Tiwary, C. S.; Kumbhakar, P. Observation of Size-Dependent Electron−Phonon Scattering and Temperature-Dependent Photoluminescence Quenching in Triangular-Shaped Silver Nanoparticles. *Plasmonics.* **2016**, *11*, 593−600.
(48) Yi, Z.; Huang, W.; Xu, Y. Dual-Emitting Zif-8⊃4-Mu@Zn2geo4:Mn2+ Nanocomposites for Ratiomertic Luminescent Thermometer and Information Encryption. *Dyes Pigm.* **2022**, *205*, 110522.
(49) Kumbhakar, P.; Roy Karmakar, A.; Das, G. P.; Chakraborty, J.; Tiwary, C. S.; Kumbhakar, P. Reversible Temperature-Dependent Photoluminescence in Semiconductor Quantum Dots for the Development of a Smartphone-Based Optical Thermometer. *Nanoscale.* **2021**, *13*, 2946−2954.
(50) Ramalho, J. F. C. B.; Dias, L. M. S.; Fu, L.; Botas, A. M. P.; Carlos, L. D.; Carneiro Neto, A. N.; André, P. S.; Ferreira, R. A. S. Customized Luminescent Multiplexed Quick-Response Codes as Reliable Temperature Mobile Optical Sensors for Ehealth and Internet of Things. *Adv. Photonics.* **2022**, *3*, 2100206.
(51) Siriwardana, K.; Nettles, C. B.; Vithanage, B. C. N.; Zhou, Y.; Zou, S.; Zhang, D. On-Resonance Fluorescence, Resonance Rayleigh Scattering, and Ratiometric Resonance Synchronous Spectroscopy of Molecular- and Quantum Dot-Fluorophores. *Anal. Chem.* **2016**, *88*, 9199−9206.
(52) Nettles, C. B.; Hu, J.; Zhang, D. Using Water Raman Intensities to Determine the Effective Excitation and Emission Path Lengths of Fluorophotometers for Correcting Fluorescence Inner Filter Effect. *Anal. Chem.* **2015**, *87*, 4917−4924.
(53) Gillispie, G. D.; Lim, E. C. T2→T1 Fluorescence in Substitute Anthracenes. *J. Chem. Phys.* **1976**, *65*, 2022−2023.
(54) Tanaka, M.; Tanaka, I.; Tai, S.; Hamanoue, K.; Sumitani, M.; Yoshihara, K. Temperature Dependence of the Nonradiative Relaxation Process of the Lowest Excited Singlet States of Meso-Substituted Bromoanthracenes. *J. Phys. Chem.* **1983**, *87*, 813−816.
(55) Hamanoue, K.; Nakayama, T.; Ikenaga, K.; Ibuki, K. Temperature Effect on the Formation of the Lowest Excited Triplet States of 9-Bromoanthracene and 9,10-Dibromoanthracene. *J. Photochem. Photobiol., A* **1993**, *74*, 147−152.

https://doi.org/10.1021/acsmeasuresciau.2c00047
ACS Meas. Sci. Au 2023, 3, 10−20